Electromagnetic and Semiconductor Device Simulation Using Interpolating Wavelets

Sebastien Goasguen, *Student Member, IEEE,* Mahmoud Munes Tomeh, and Samir M. El-Ghazaly, *Fellow, IEEE*

***Abstract*—A MESFET and a two-dimensional cavity enclosing a cylinder are simulated using a nonuniform mesh generated by an interpolating wavelet scheme. A self-adaptive mesh is implemented and controlled by the wavelet coefficient threshold. A fine mesh can therefore be used in domains where the unknown quantities are varying rapidly and a coarse mesh can be used where the unknowns are varying slowly. It is shown that good accuracy can be achieved while compressing the number of unknowns by 50% to 80% during the whole simulation. In the case of the MESFET, the I–V characteristics are obtained and the accuracy is compared with the basic finite difference scheme. A reduction of 83% in the number of discretization points at steady state is obtained with 3% error on the drain current. The performance of the scheme is investigated using different values of threshold and two types of interpolating wavelet, namely, the second-order and fourth-order wavelets. Due to the specific problem analyzed here, a tradeoff appears between good compression, accuracy, and order of the wavelet. This represents the ongoing effort toward a numerical technique that uses wavelets to solve both Maxwell's equations and the semiconductor equations. Such a method is of great interest to deal with the multiscale problem that is the full-wave simulation of an active microwave circuits.**

***Index Terms*—Adaptive gridding, global modeling, microwave circuits, multiresolution, thresholding, time-domain method, wavelets.**

I. Introduction

WITH THE increasing flow of data in the telecommunication world, the performances of high-frequency devices have become more demanding. Typical circuit simulators no longer represent the accurate tool to characterize microwave circuits. Electromagnetic (EM) simulators need to be used to tackle the problems of EM interference such as packaging effects and coupling between subcircuits among others.

The full-wave analysis of microwave circuits (global modeling) is a tremendous task that requires involved numerical techniques and algorithms. In [1], the authors self-consistently solve Maxwell's equations together with the semiconductor equations that characterize a submicrometer gate device. Alternative techniques have shown interesting results. The extended finite-difference time-domain (FDTD) method [2] that can deal with an equivalent circuit of the active device has been used to predict nonlinear phenomena and electromagnetic compatibility (EMC) effects [3]. A hybrid technique using the frequency-domain finite-element method and a circuit simulator has also demonstrated good capability to predict the behavior of different transistor topology using the same process [4]. Those techniques, however, cannot simulate the propagation effects occurring inside the transistor at very high frequencies. Therefore, it is our belief that there is an urgent need to present a new approach to the computational problem of global modeling to make this technique practical for circuit design at millimeter waves.

On one hand, one can decide to use the FDTD technique to solve for the EM fields of the passive and active parts, but soon will face a difficult problem. The cell size of passive parts will be almost as big as the whole transistor. Therefore, computationally expensive techniques like time-domain diakoptics must be employed [1], [5]. On the other hand, implementing a technique that adaptively refines the mesh in domains where the unknown quantities vary rapidly would considerably reduce the number of unknowns. Such a technique corresponds to a multiresolution analysis of the problem. A very attractive way of implementing a multiresolution analysis is to use wavelets [6]. Wavelets have been used in electromagnetics for a few years, first in the method of moments [7] and later in FDTD. It was demonstrated [8] that finite-difference schemes can be derived using the method of moments with wavelet expansions of the fields. The resulting numerical technique has been called the multiresolution time-domain technique (MRTD) [9]. This method has been studied extensively [10] and shows very good performance as for the accuracy, memory requirements, and CPU time. Nevertheless, the implementation of wavelets to semiconductor equations is still to be investigated thoroughly in order to determine if a multiresolution numerical method can be used in the context of global modeling. The MRTD can be regarded as a wavelet-based Galerkin method. For nonlinear equations such as semiconductor modeling equations, this method can become quite time consuming [11]. Therefore, in this paper, a different wavelet approach is investigated, bearing in mind the possible hybridization of different multiresolution techniques in the future. We propose to apply a wavelet interpolating scheme to the semiconductor equations and Maxwell's equations. The equations are solved on a dyadic grid. The wavelet coefficients are directly related to the physical domain as they represent the error between the exact solution on the grid and the interpolated value from the previous coarser mesh. This scheme allows us to multiply and differentiate very

Manuscript received April 3, 2001; revised August 24, 2001. This work was supported by the U.S Army Research Office under Contract DAAD19-99-1-0194 and by the Semiconductor Research Corporation under Contract 99-NJ-719.

S. Goasguen is with the Electrical and Computer Engineering Department, Purdue University, West Lafayette, IN 47907 USA (e-mail: sebgoa@purdue.edu).

M. M. Tomeh is with Micro Photonix Integration Corporation, Phoenix, AZ 85029 USA (e-mail: M_Tomeh@mpi-ioc.com).

S. M. El-Ghazaly is with the Telecommunications Research Center, Arizona State University, Tempe, AZ 85287 USA (e-mail: sme@asu.edu).

Publisher Item Identifier S 0018-9480(01)10470-9.

Fig. 1. Three dyadic grids.

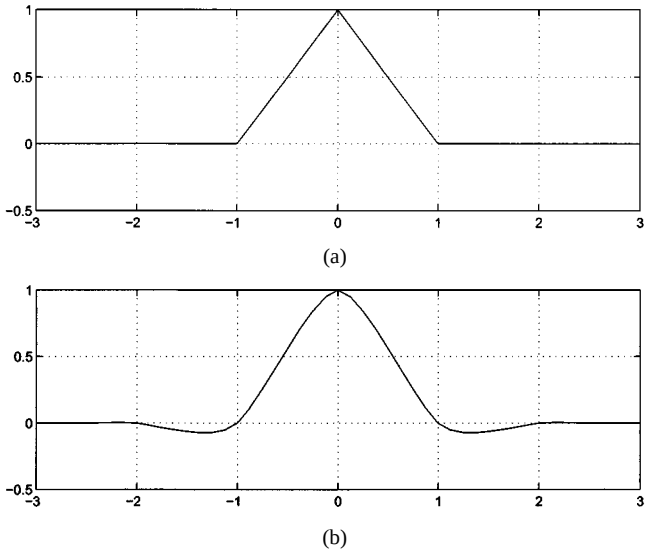

Fig. 2. Scaling function for: (a) $p = 2$ and (b) $p = 4$.

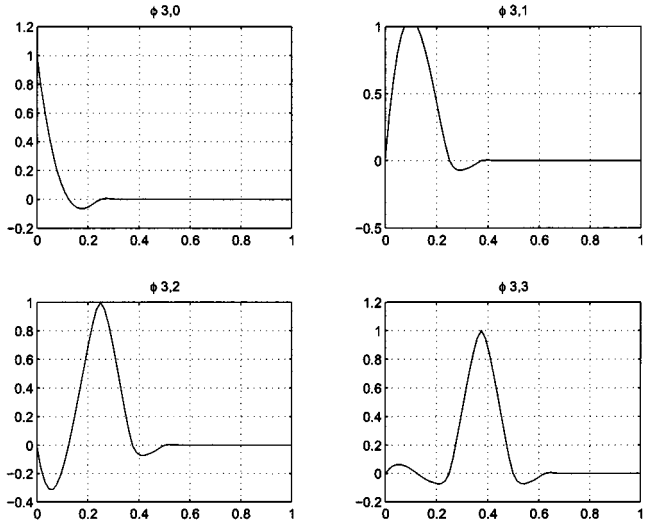

Fig. 3. Left boundary scaling function for $p = 4$.

Fig. 4. Wavelet subspaces representation.

quickly. We will follow the algorithm explained in [12] that has been used to solve one-dimensional (1-D) Maxwell's equations in [13] and a two-dimensional (2-D) p-n junction in [14]. We will use this scheme to solve a 2-D cavity (TE case) enclosing a cylinder representing a discontinuity inside the cavity. This cylinder will allow us to see the refinement process that occurs during the simulation. We will also present the simulation of a typical MESFET.

This paper is organized as follows. Section II gives an introduction to the interpolating wavelet and the numerical scheme used to solve the partial differential equations (PDEs). Section III presents a brief review of the MESFET physical models in the context of global modeling. Numerical experiments done on a 2-D cavity and a drift-diffusion model are related in Section IV together with the investigation of the numerical scheme performance. Finally, conclusions are drawn in Section V.

II. Interpolating Wavelet Scheme

The wavelet scheme is based on the interpolating subdivision scheme studied by Deslauriers and Dubuc [15]. It was later extended in an interpolated wavelet transform by Donoho [16]. The idea is to consider a set of dyadic grids that defines different resolution levels. A grid contains all points of the coarser level plus points inserted halfway between those. Values at odd grid points are kept unchanged while values at even points are interpolated by a polynomial. The set of dyadic grids can be represented as shown in Fig. 1.

If we start on the coarser grid with the Kronecker delta function and interpolate the values at even grid points, we build the scaling function. According to the order of the interpolating polynomial, the scaling function built is different. Fig. 2 shows the scaling function for two different type of interpolation, linear interpolation $p = 2$ and cubic interpolation $p = 4$. This scaling function is defined on the real line so special attention should be given to the boundaries. In the case of linear interpolation, the scheme remains the same, but for other polynomials ($p = 4$), the standard stencil must be modified. Fig. 3 shows the left boundary scaling functions for level 3 when $p = 4$. Interestingly enough, this scaling function φ is the autocorrelation function of the Daubechies wavelet [17]. For a given order p, $\varphi(x) = \int \tilde{\varphi}(y)\tilde{\varphi}(y - x)\,dy$ where $\tilde{\varphi}$ is the scaling function associated with Daubechies wavelets of $p/2$ vanishing moments. It was shown in [18] that the expansion of the solution of an elliptic PDE in terms of interpolating scaling function leads to the same linear system than the one obtained by using Daubechies wavelets as test and trial function in a Galerkin method. From construction, this scaling function has a compact support $[-p + 1, p - 1]$ and verifies the dilation equation specific to wavelets

$$\varphi(x) = \sum_{k=-p+1}^{k=p-1} g_k \varphi(2x - k).$$

This scaling function is used to refine the mesh, in other terms move from subspace V_j to subspace V_{j+1}. We can introduce subspace W_j to define the difference between V_j and V_{j+1}. These new subspaces can be represented as shown in Fig. 4.

A possible choice of functions that span the subspaces W_j is the set of scaling functions itself. Therefore, it defines a nonorthogonal multiresolution. In this representation, the wavelet coefficients are the error between the value at odd grid points and the interpolated value at a coarser grid. With this wavelet representation, one can refine or coarsen the mesh as desired.

Now we can create the so-called sparse point representation of a function f [12]. Starting with the coarsest grid, we create an irregular mesh by computing the error between the exact value of f on the coarse grid and the value obtained by interpolation. The wavelet coefficients carry the detailed signal: the error between the exact value and the interpolated value. By removing the points that can be interpolated, we greatly compress the data defining a sparse point representation (SPR) that can be used for computation. The number of points remaining in the SPR depends on the smoothness of the function. If the function varies smoothly, it will be easily described by a polynomial interpolation and thus the SPR will contain very few points. If the function varies rapidly, then the SPR will contain more points as the interpolation will be insufficient to coarsen the mesh. The compression that one can obtain depends on the threshold value set as the minimum error for the interpolation procedure.

This extremely versatile technique is expected to be very useful to solve PDEs, especially nonlinear ones. Multiplication and derivatives can be computed in this SPR, which may considerably reduce the computation time. The typical way of solving a PDE using the SPR representation is to transform the PDE into a system of ordinary differential equations (ODEs) using the method of lines. The initial conditions are set and the first SPR is obtained, the spatial derivatives are approximated using the interpolated wavelet scheme [12], and the new time iteration is performed using an ODE solver. The type of PDE that is to be solved may introduce some changes in the algorithm, as the SPR may not need to be computed at each time step. The ODE solver also offers a great degree of freedom as one can choose between standard Runge–Kutta methods, multistep methods, and so on. In general, the more expensive the ODE solver, the more efficient this scheme will be as the overhead created by the SPR manipulation will be overcome by the spatial derivatives approximations. In summary, the algorithm to solve a differential equation using this scheme is as follows:

- set initial conditions;
- obtain the SPR of the unknowns;
- approximate spatial derivative using SPR interpolation;
- advance in time using ODE solver;
- go back to the SPR computation.

A similar scheme has been employed to solve the problem of a 2-D p-n junction [14]. However, in this previous work, the electron and hole mobilities were assumed constant. This assumption severely limits the validity of the technique for simulating modern semiconductor devices used for high-speed or high-frequency applications. Therefore, in this paper, we propose to treat the problem of a field-effect transistor with mobility and diffusion coefficient as functions of the electric field.

III. MESFET Physical Model

In the context of global modeling, the active devices simulated are submicrometer gate devices that exhibit the hot electron phenomena with a 2-D distribution of the energy [19]. The physical model used is called the full hydrodynamic model and is based on the moments of the Boltzmann's transport equations obtained by integration over the momentum space. These equations provide a time-dependent solution for carrier density, energy, and momentum. They are given as follows.

- Current continuity

$$\frac{\partial n}{\partial t} + \nabla \cdot (nv) = 0.$$

- Energy conservation

$$\frac{\partial (n\varepsilon)}{\partial t} + \nabla .(nv\varepsilon) = qnv.E - \nabla .(nkTv) - \frac{n(\varepsilon - \varepsilon_0)}{\tau_\varepsilon}.$$

- Momentum conservation

$$\frac{\partial (np_x)}{\partial t} + \nabla .(np_x v) = qnE_x - \nabla (nkT) - \frac{np_x}{\tau_m}$$

where n is the electron concentration, v the electron velocity, E the electric field, and p the momentum. In the energy conservation equation, ε represents the electron energy and ε_0 is the equilibrium thermal energy (in all sections of the paper, ε refers to the wavelet coefficient threshold or the dielectric constant). The time and spatial dependencies are not neglected to appropriately model submicrometer gate devices RF and transient conditions. In the early stage of this work, we need to demonstrate that the interpolating wavelet scheme can be used to solve semiconductor equations and that it will bring versatility and efficiency in the numerical technique used for global modeling. As a result, a simplifying assumption is made in this paper and the drift diffusion model is considered to obtain the behavior of the active device. Ultimately, a full hydrodynamic model should be implemented with Maxwell's equations to obtain a self-consistent simulation of the propagation effects in sub-micrometer gate devices. The equations to be solved in the drift-diffusion model for a unipolar device are

- Poisson's equations

$$-\nabla^2 \Psi = \frac{q}{\varepsilon}(N - n),$$

- continuity equation

$$\frac{\partial n}{\partial t} = \nabla \cdot J_n,$$

with

$$J_n = \mu_n \cdot n \cdot E + D_n \cdot \nabla n$$

where N is the doping profile, n the electron density, and μ_n and D_n are the mobility and the diffusion coefficient, respectively. As it was said before, in a previous work [14] they were assumed to be constants. In this work, they are functions of the electric field. The mobility is defined by an empirical formula

$$\mu(E) = 2\mu_0 \left\{ 1 + \left[1 + \frac{2\mu_0 E}{v_\infty} \right]^{1/2} \right\}^{-1}$$

where μ_0 is the zero-field mobility and ν_∞ is the saturation velocity. The diffusion term is also a function of the electric field thanks to the mobility. The diffusivity is defined by the Einstein relation

$$D = \frac{kT}{q}\mu$$

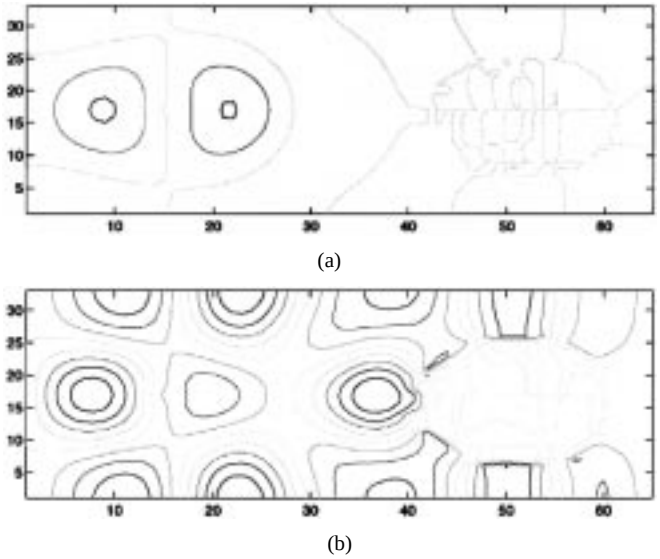

Fig. 5. Electric field in the y direction. (a) $t = 520$ ps. (b) $t = 840$ ps.

where T is the temperature and k the Boltzmann's constant. Poisson's equations can be discretized by finite-difference schemes. This results in a linear system that can be solved by any iterative solver provided that the matrix representation of the discretized operator satisfies the stability and convergence criteria such as positive definite matrix. As the Poisson's equations is to be replaced in a future work by the Maxwell's equations, no significant efforts were put to gain computational time while solving this equation. All the effort was concentrated on the continuity equation that exhibit nonlinearity. However, as mentioned in the previous section, a discretization of Poisson's equation using Daubechies wavelets leads to the same system as the one obtained by interpolating scaling functions [18]. The continuity equation is solved using the interpolating scheme presented in the previous section. Time-domain simulations are performed. One can verify that the gate current is zero as effectively no current must flow through the Schottky contact. A relative error is defined in order to compare the standard finite-difference method that uses a uniform mesh and the interpolating wavelet scheme that generates the nonuniform mesh. This relative error is defined on the drain current as

$$e_{\text{relative}} = \frac{\|J_\varepsilon - J_{\text{FD}}\|}{\|J_{\text{FD}}\|}$$

where J_ε is the drain current density computed by the interpolating wavelet scheme using a threshold of ε on the SPR of the carrier density and J_{FD} is the drain current density computed by a standard finite-difference code.

IV. Results

Initial results of MESFET simulation were introduced in [20]. A 2-D cavity is now simulated according to the example presented in [21]. The cavity is discretized by a mesh of $65 * 33$ with a space increment $dx = 3.0$ mm. The time increment is $dt = 5.0$ ps. Fig. 5 shows the y component of the electric field at two different time. We can see that at $t = 520$ ps the wave did not reach the cylinder yet, whereas at $t = 840$ ps the modes

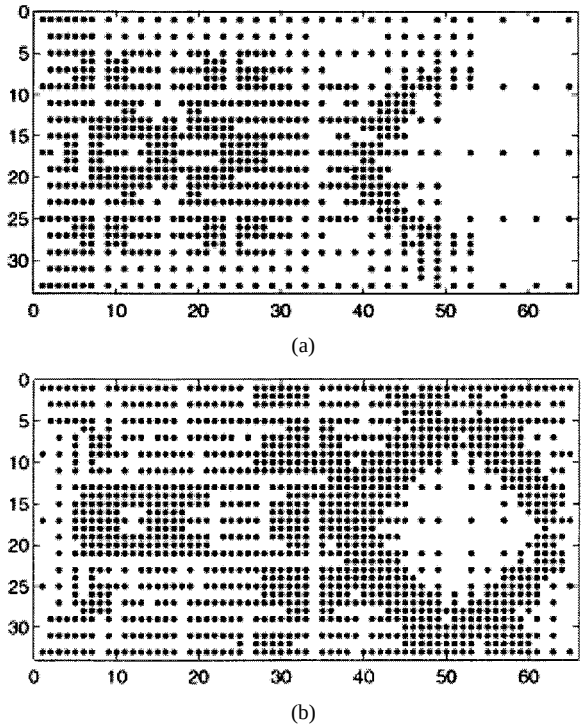

Fig. 6. SPR of the y component of the electric field at: (a) $t = 520$ ps and (b) $t = 840$ ps.

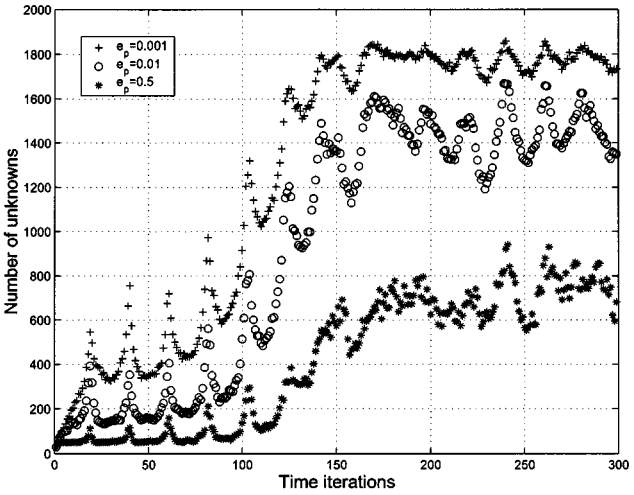

Fig. 7. Number of unknowns remaining in the SPR for three different values of wavelet threshold.

inside the cavity are developing and scattering due to cylinder is occurring.

Fig. 6 shows the SPR or, in other terms, the nonuniform mesh generated by the scheme at the same time as in Fig. 5. This demonstrates the self-adaptibility of the mesh which gets finer in regions where the fields are varying rapidly. At $t = 840$ ps, scattering due to the cylinder needs to be modeled accurately; therefore, more points are used around the cylinder. At every time step, this nonuniform mesh is generated by the wavelet scheme. Thus, the number of unknowns varies in time. Fig. 7 shows this behavior. Three wavelet thresholds are used. We can see that, as the threshold gets smaller, more points need to be used in the mesh. The error computed during the interpolation

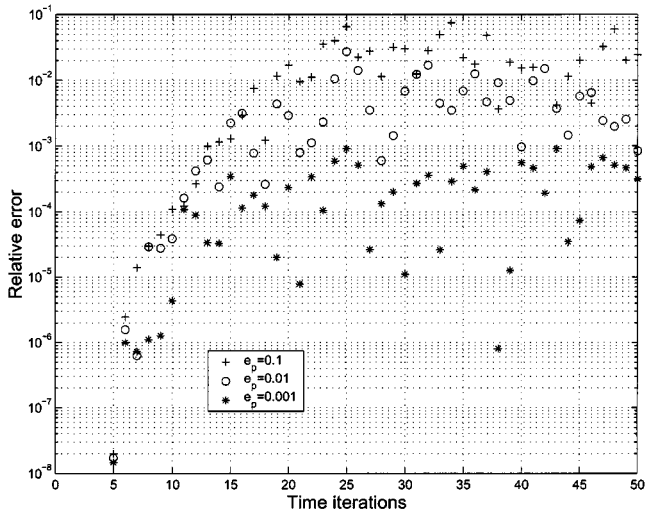

Fig. 8. Relative error of the electric field versus time for three wavelet threshold values.

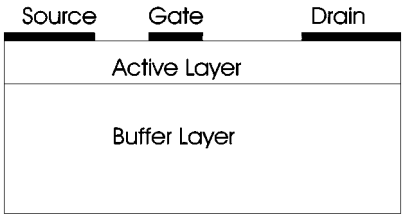

Fig. 9. 2-D conventional structure of the simulated MESFET.

needs to be smaller, thus finer mesh are used. These results were compared with the FDTD results from [21]. Fig. 8 shows the relative error on the electric field versus time. A random point was chosen within the structure to record the values of the electric field, then the relative error was computed every six time steps. The adaptability of the mesh makes the error extremely dependent on time. However, it can be seen that the error is reduced as the wavelet threshold is minimized. This is an expected behavior due to the fact that, when the threshold is minimized, the grid is refined and looks more like the finite-difference grid used in [21].

Then, a MESFET with the following dimensions is simulated: 0.6-μm gate length, 1-μm-long source and drain electrodes, 0.7-μm source–gate gap, 1.5-μm gate–drain separation, 0.2-μm-deep channel layer, and a 0.8-μm-deep buffer layer. Fig. 9 presents the conventional 2-D structure used for simulations. The doping of the active layer is 1.2×10^{17} A/cm^3 and the doping of the buffer layer is 1×10^{14} cm^{-3}. The zero-field mobility is 800 cm^2/V$\cdot$s and the saturation velocity ν_∞ is 10^7 cm/s. A $65 * 65$ mesh was used for spatial discretization while the Euler's method was used as the ODE solver. The time step was chosen to be 8.10^{-15} s, but due to the nonuniform meshes used some tuning was required to ensure stability. Fig. 10 shows the I–V characteristics of the simulated MESFET. A typical behavior is observed. The electrostatic potential contour plot is shown in Fig. 11 for a drain voltage of 2 V and a gate voltage of -1 V. In Fig. 12, the carrier distribution is plotted and the corresponding SPR can be compared in Fig. 13 for the same bias condition as the potential

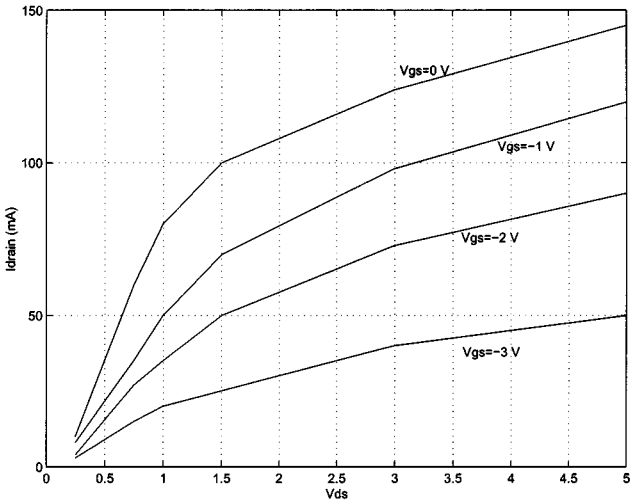

Fig. 10. I–V characteristics of the simulated MESFET.

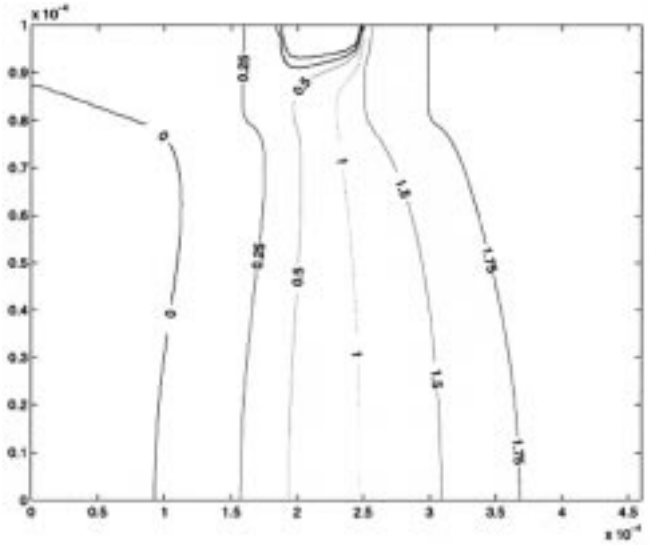

Fig. 11. Contour plot of the electrostatic potential for a drain voltage of 2 V and an applied external gate voltage of -1 V.

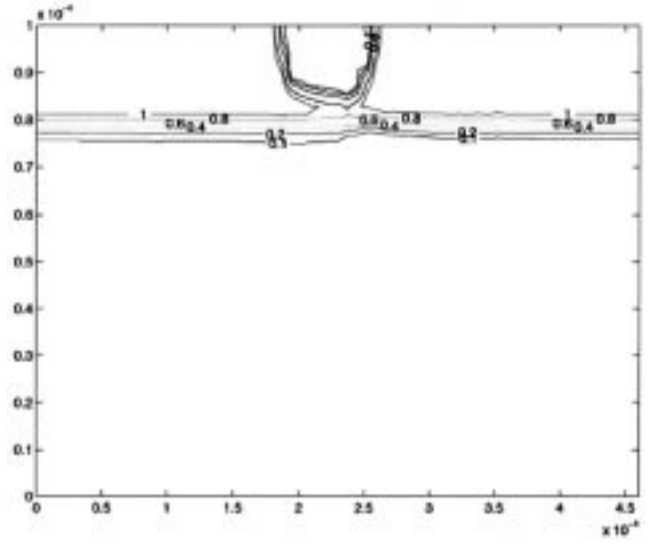

Fig. 12. Contour plot of the carrier density (the labels are normalized by 10^{17}) for 2-V drain voltage and -1-V applied gate voltage.

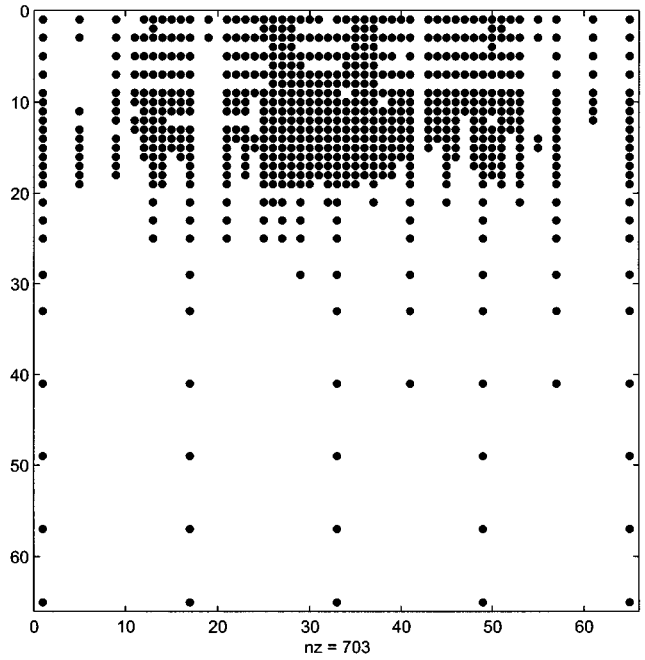

Fig. 13. SPR of the carrier density at 2-V drain voltage and −1-V applied gate voltage.

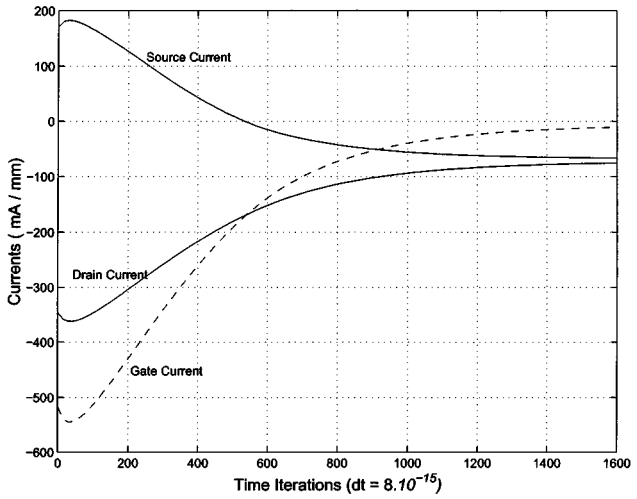

Fig. 14. Time-domain drain, source, and gate currents at 2-V drain voltage and −1-V applied gate voltage.

shown in Fig. 11. We observe that the depletion region was created in the channel. The SPR kept mesh points in the grid where the carrier density varies rapidly, namely, around the depletion region and along the junction between the channel and the buffer layer. In smooth regions, where the interpolation is more accurate, fewer points are needed. Thus, few points are necessary to predict the carrier density deep in the buffer layer. This representation changes in time, which makes the grid dynamically adaptive.

The performance of the new scheme is investigated at a single bias point: 2-V drain voltage and −1-V applied gate voltage. Fig. 14 shows the drain, source, and gate currents computed at each time step. A conventional behavior is obtained as the source and drain currents converge to the same value and the gate current tends to zero. Three absolute wavelet thresholds

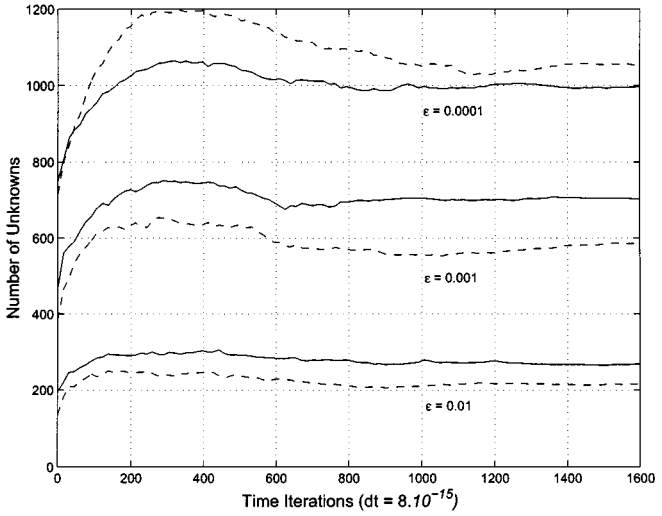

Fig. 15. Mesh adaptability for three different values of wavelet threshold. (Solid lines: $p = 2$; dashed lines: $p = 4$).

were chosen: $\varepsilon = 0.01$, $\varepsilon = 0.001$, and $\varepsilon = 0.0001$. The relative threshold was defined as $\varepsilon.N_d$, where N_d is the doping of the channel layer. A set of simulations was performed for these three threshold values and for two cases of scaling functions $p = 2$ and $p = 4$. Fig. 15 represents the number of mesh points remaining in the SPR after thresholding of the wavelet coefficients. Different conclusions can be drawn from this numerical experiment. As the threshold gets smaller, the error that is tolerated in the representation of the carrier density gets smaller, and more points are necessary to accurately represent the carrier density. At the beginning of the simulation, the carrier density is initialized to the doping profile, thus very few points are needed due to the smoothness of this initial condition. As time evolves, the depletion region starts to appear and points are added in the SPR, which is why, for the first 400 iterations, the number of unknowns grows. When the depletion region is created and the MESFET starts to reach its steady state, the carrier concentration stops changing and the number of points in the SPR remains the same.

These above remarks illustrate the dynamic behavior of the mesh. More involved is the behavior of the SPR for $p = 2$ and $p = 4$. Fig. 15 demonstrates that, for $\varepsilon = 0.01$ and $\varepsilon = 0.001$, the linear interpolation achieves a better compression ratio than the cubic interpolation. For $\varepsilon = 0.0001$, however, it is the opposite. When the carrier density is almost constant, the linear interpolation performs better. Only two points can be used to describe the correct solution: the coarser mesh of the linear interpolation requires fewer points than the cubic interpolation. In the depletion region where the carrier density varies rapidly, a significant error is acceptable. So, the linear interpolation still uses less unknowns than the cubic one. At $\varepsilon = 0.0001$, it appears that the breaking point has been reached, and the linear interpolation can no longer describe the depletion region with the required accuracy without using the finest mesh. It is our understanding that this breaking point is a function of the wavelet threshold, the bias point, and the physical dimensions. The buffer layer can be made smaller, which would result in a depletion region occupying more space in the computational

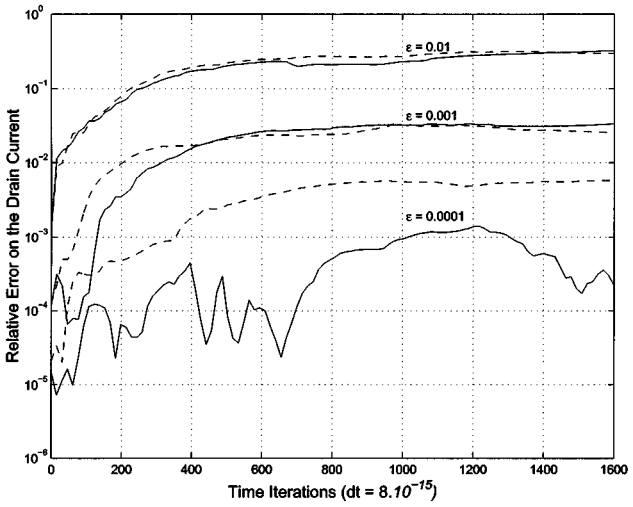

Fig. 16. Relative error on the drain current for three different values of wavelet threshold. (Solid lines: $p = 2$; dashed lines: $p = 4$).

domain. The cubic interpolation could therefore outperform the linear one for a much bigger error than is the case in this experiment. Finally, Fig. 16 presents the relative error defined in the previous section. This graph compares the solution of a standard finite-difference scheme, using uniform mesh, with the interpolating scheme. Once again, the results are plotted for three wavelet thresholds and the two previous interpolating scaling functions. For the two cases $\varepsilon = 0.01$ and $\varepsilon = 0.001$, the error on the drain current is, respectively, 50% and 5%, and there is no major difference between the two scaling functions. This shows that, for these given wavelet thresholds, one would choose the linear interpolation to achieve better CPU time. In the case of $\varepsilon = 0.0001$, the linear interpolation gives a relative error of 0.8% while the cubic interpolation gives an error of 0.1%. These results help to determine how to choose the wavelet threshold.

In this study, we also examined the computational overhead created when the SPRs are generated. On the one hand, this scheme shows good promises with a potential reduction in the computation time between 74% to 95%. On the other hand, the overhead currently reduces the gain in computation time to a range of 25% to 55% for the different thresholds presented earlier. An appropriate data structure is expected to improve those performances. It is also to be noted that more computationally expensive ODE solvers could be used which would reduce the share of CPU time used to deal with the SPRs. The initial size of the mesh that defines the finest grid also affects the CPU time performances of the scheme because the size of the system of ODE changes.

V. Conclusion

A wavelet approach based on an interpolation scheme has been used to solve the two sets of PDEs, namely, Maxwell's equations for EM analysis and the drift-diffusion model for the field-effect transistor analysis. In the FET simulation, a reduction of 83% in the number of unknowns is obtained while keeping the I–V characteristics in an acceptable 3% of accuracy relative to a conventional finite-difference scheme. For EM simulation, similar results can be achieved. The reduction in CPU time is a function of the ODE solver. The overhead created by generating the nonuniform mesh can be reduced by an appropriate data structure and can be negligible compared to the number of times the SPRs are used in the ODE solver. This opens the door to an efficient numerical technique suitable for global modeling of microwave circuits. This scheme will be applied to more complex semiconductor models in the near future to model the particle-wave interaction that occurs inside high-frequency and high-speed active devices.

References

[1] S. M. S. Imtiaz and S. M. El-Ghazaly, "Global modeling of millimeter-wave circuits: Electromagnetic simulation of amplifiers," *IEEE Trans. Microwave Theory Tech.*, vol. 45, pp. 2208–2216, Dec. 1997.

[2] W. Sui, D. A. Christensen, and C. H. Durney, "Extending the two-dimensional FDTD method to hybrid electromagnetic systems with active and passive lumped elements," *IEEE Trans. Microwave Theory Tech.*, vol. 40, pp. 724–730, Apr. 1992.

[3] K-P. Ma, B. Housmand, Y. Qian, and T. Itoh, "Global time-domain full-wave analysis of microwave circuits involving highly nonlinear phenomena and EMC effects," *IEEE Trans. Microwave Theory Tech.*, vol. 47, pp. 859–866, June 1999.

[4] E. Larique *et al.*, "Linear and nonlinear FET modeling applying an electromagnetic and electrical hybrid software," *IEEE Trans. Microwave Theory Tech.*, vol. 47, pp. 915–918, June 1999.

[5] T-W. Huang, B. Houshmand, and T. Itoh, "The implementation of time-domain diakoptics in the FD-TD method," *IEEE Trans. Microwave Theory Tech.*, vol. 42, pp. 2149–2155, Nov. 1994.

[6] S. G. Mallat, "A theory for multiresolution signal decomposition: The wavelet representation," *IEEE Trans. Patt. Anal. Machine Intell.*, vol. 11, pp. 674–693, July 1989.

[7] B. Z. Steinberg and Y. Leviatan, "On the use of wavelet expansions in the method of moments," *IEEE Trans. Antennas Propagat.*, vol. 41, pp. 610–619, May 1993.

[8] M. Krumpholz and L. P. B. Katehi, "MRTD: New time-domain schemes based on multiresolution analysis," *IEEE Trans. Microwave Theory Tech.*, vol. 44, pp. 555–571, Apr. 1996.

[9] M. Tentzeris, J. Harvey, and L. P. B. Katehi, "Time adaptive time-domain techniques for the design of microwave circuits," *IEEE Microwave Guided Wave Lett.*, vol. 9, pp. 96–99, Mar. 1999.

[10] L. P. B. Katehi, J. Harvey, and E. Tentzeris, "Time-domain analysis using multiresolution expansions," in *Computational Electrodynamics*, A. Taflove, Ed. Norwood, MA: Artech House, 1995.

[11] J. Keiser, "Wavelet based approach to numerical solution of nonlinear partial differential equations," Ph.D. dissertation, Dept. Math., Univ. Colorado, Boulder, CO, 1995.

[12] M. Holmstrom, "Solving Hyperbolic PDE's Using Interpolating Wavelets," Dept. Sci. Comput., Uppsala Univ., Uppsala, Sweden, Dec. 1996.

[13] G. Rubinacci *et al.*, "Interpolating wavelets for the solution of Maxwell equations in the time domain," *IEEE Trans. Magn.*, vol. 34, pp. 2775–2778, Sept. 1998.

[14] M. Toupikov, G. Pan, and S. M El-Ghazaly, "Global modeling of microwave devices using wavelets," in *IEEE MTT-S Int. Microwave Symp. Dig.*, vol. 1, Baltimore, MD, June 1998, pp. 263–266.

[15] G. Deslauriers and S. Dubuc, "Symmetric iterative interpolation processes," *Construc. Approxim.*, vol. 5, no. 1, pp. 49–68, 1989.

[16] D. L. Donoho, "Interpolating wavelet transforms," Dept. Stat., Stanford Univ., Stanford, CA, Tech. Rep. 408, Nov. 1992.

[17] N. Saito and G. Beylkin, "Multiresolution representations using the auto-correlation functions of compactly supported wavelets," *IEEE Trans. Signal Processing*, vol. 4, pp. 381–384, Jan. 1992.

[18] S. Bertoluzza and G. Naldi, "A wavelet collocation method for the numerical solution of partial differential equations," *Appl. Comput. Harmon. Anal.*, vol. 3, pp. 1–9, 1996.

[19] C. M. Snowden and D. Loret, "Two-dimensional hot electron models for short gate-length GaAs MESFET's," *IEEE Trans. Electron Devices*, vol. ED-34, no. 2, pp. 212–223, Aug. 1987.

[20] S. Goasguen and S. M. El-Ghazaly, "Interpolating wavelet scheme toward global modeling of microwave circuits," in *IEEE MTT-S Int. Microwave Symp. Dig.*, vol. 1, Boston, MA, June 2000, pp. 375–378.

[21] A. Taflove, *Computational Electrodynamics*, 2nd ed. Norwood, MA: Artech House, 1999.

Sebastien Goasguen (S'01) was born on March 22, 1974, in Rennes, France. He received the B.S. degree in electrical engineering from the Polytechnic Institute of Toulouse, Toulouse, France, in 1997, the M.S. degree (with honors) in electronics research from the King's College, London, U.K., in 1998, and the Ph.D. degree from Arizona State University, Tempe, in 2001.

His area of research is large and ranges from linearization techniques and monolithic-microwave integrated-circuit (MMIC) design to numerical techniques and semiconductor modeling. In September 2001, he began a full-time post-doctoral position with the Electrical and Computer Engineering Department, Purdue University, West Lafayette, IN, where he is involved in nanotechnology and molecular electronics.

Mahmoud Munes Tomeh received the B.A. degree in physics from the University of California at Berkeley, in 1995, and is currently working toward the M.S. degree in electrical engineering at Arizona State University, Tempe.

In 1999, he joined the Microwave Circuits Laboratory, Arizona State University, as a Research Assistant.

Samir M. El-Ghazaly (S'84–M'86–SM'91–F'01) received the Ph.D. degree in electrical engineering from the University of Texas at Austin, in 1988.

In August 1988, he joined the Arizona State University, Tempe, where he is currently a Professor in the Department of Electrical Engineering. He has visited and worked at several universities and research centers, including Cairo University, Cairo, Egypt, the Centre Hyperfrequences et Semiconducteurs, Université de Lille I, Lille, France, the University of Ottawa, Ottawa, ON, Canada, the University of Texas at Austin, the NASA Jet Propulsion Laboratory, Pasadena, CA, CST–Motorola Inc., Tempe, AZ, *iemn*, Université de Lille, Lille, France, and the Swiss Federal Research Institute (ETH), Zurich, Switzerland. His research interests include RF and microwave circuits and components, microwave and millimeter-wave semiconductor devices, semiconductor device simulations, ultrashort pulse propagation, microwave-optical interactions, linear and nonlinear modeling of superconductor microwave lines, wave–device interactions, electromagnetics, and numerical techniques applied to monolithic microwave integrated circuits.

Dr. El-Ghazaly is a Fellow of IEEE. He is an elected member of Commissions A and D of URSI, and a member of Tau Beta Pi, Sigma Xi, and Eta Kappa Nu. He was the secretary and vice-chairman and is currently the chairman of Commission A of the U.S. National Committee of URSI. He is a member of the Technical Program Committee for the IEEE IMS since 1991, and is on the Editorial Board of the IEEE TRANSACTIONS ON MICROWAVE THEORY AND TECHNIQUES. He was the chairman of the IEEE Waves and Devices Group, Phoenix Section. He was the chapter funding coordinator and chairman of the Chapter Activities Committee of the IEEE MTT-S. He is an elected member of the AdCom of the IEEE MTT-S. He is the editor-in-chief for the IEEE MICROWAVE AND WIRELESS COMPONENTS LETTERS. He was the general chairman of the IEEE MTT-S 2001 IMS, held in Phoenix, AZ, May 2001.